15th ASCE Engineering Mechanics Conference
June 2-5, 2002, Columbia University, New York, NY

THREE DIMENSIONAL MODELING OF SLIP SURFACES IN GEOMATERIALS

Richard A. Regueiro[1], Member, ASCE
Craig D. Foster[2], Member, ASCE
Ronaldo I. Borja[3], Member, ASCE

ABSTRACT

A three-dimensional finite element implementation of a simple nonassociative Drucker-Prager plasticity model with strong discontinuity mode of localized deformation is formulated for small deformations. A strong discontinuity mode of localized deformation represents slip along a surface of zero measure, whereas a weak discontinuity mode of localized deformation represents shear within a band of finite thickness. A numerical algorithm that detects onset of localization for three-dimensional stress states and the possible normals to slip planes within a three-dimensional finite element is demonstrated. An enhanced strain hexahedral finite element accounting for the various slip-plane cutting conditions is described. This model and finite element lead to mesh-independent solutions with regard to mesh refinement and mesh alignment. A simple three dimensional numerical example demonstrates the numerical algorithm for determining onset of localization.

Keywords: localized deformation, slip surfaces, pressure-sensitive materials, strong discontinuity plasticity

INTRODUCTION

Localized deformation in the form of slip surfaces appears in rock (Wawersik et al. 1990) and heavily overconsolidated clays (Hvorslev 1960, Atkinson 1993) for certain loading conditions. Many modeling approaches such as fracture mechanics, plasticity, and damage have been proposed to represent slip surfaces in geomaterials and the associated loss of material strength. For geomaterials, "plasticity" implies phenomenological inelastic material behavior due to granule rotation and translation within (or without) the matrix material, granule crushing, clay platelet deformation and motion, and micro-cracking in rock, for instance, as opposed to plasticity in polycrystalline materials (such as metals) that implies dislocation motion, storage, and annihilation as well as possibly twinning. Given the scale of geomechanical problems (meters to kilometers) as well as their significant in-situ material inhomogeneity, phenomenological (or statistically-averaged micromechanical) models are appropriate. On the other hand, a phenomenological approach is not applicable to problems on the scale of microstructure (micrometers to millimeters) such as microsystems deformation or onset of ductile fracture in metals for which physically-based micromechanical nonlocal models are necessary.

[1]Science-Based Materials Modeling Dept., Sandia National Laboratories, P.O. Box 969, MS 9405, Livermore, CA, 94551-0969, E-mail: raregue@sandia.gov
[2]Dept. of Civ. & Env. Eng., Stanford University, Stanford, CA, 94305-4020, E-mail: cdfoster@stanford.edu
[3]Dept. of Civ. & Env. Eng., Stanford University, Stanford, CA, 94305-4020, E-mail: borja@stanford.edu

The strong discontinuity plasticity modeling approach was first put forth by Simo and coworkers (Simo et al. 1993, Simo and Oliver 1994, Armero and Garikipati 1996, Oliver et al. 1999) and espoused by others. It was then extended to pressure-sensitive plasticity models (Larsson et al. 1996, Armero and Callari 1999, Borja and Regueiro 2001, Regueiro and Borja 2001, Wells and Sluys 2001, Borja 2002).

This paper presents the three-dimensional extension of a previously developed small-strain, two-dimensional model of pressure-sensitive plasticity with strong discontinuity (Borja and Regueiro 2001, Regueiro and Borja 2001). Specifically, a numerical algorithm to detect onset of localization is demonstrated and an enhanced strain hexahedron with slip plane is discussed.

MODEL

A brief description of the strong discontinuity modeling approach is described within the context of a simple geomaterial constitutive model such as the small deformation, nonassociative, isotropic hardening/softening Drucker-Prager plasticity model.

The elegance of the strong discontinuity approach is that the plasticity model of interest is formulated with strong discontinuity mode of deformation, and a bifurcation condition (for rate-independent plasticity) along with the form of a post-bifurcation traction-slip-displacement relation result. Before continuing, we note that the mathematically-derived bifurcation condition lacks physical motivation because it is derived from the pre-bifurcation plasticity model and thus depends on the choice of material parameters for this model, which are typically determined from experimental data for homogeneously-deformed specimens of material. Determination of a physically-motivated bifurcation condition requires better understanding of the underlying physical mechanisms associated with onset of localized deformation in geomaterials, which is an ongoing area of interest for modelers and experimentalists at Sandia (Olsson 2000, DiGiovanni et al. 2000) as well as other institutions. This is especially relevant for rate-dependent plasticity models for which no bifurcation condition can be mathematically formulated because there is no loss of strong ellipticity of the acoustic tensor (Sandler and Wright 1984, Needleman 1988, Armero 1999, Wells et al. 2002).

Kinematics of strong discontinuity

The formulation of a plasticity model with strong discontinuity mode of deformation begins with an additative decomposition of the velocity field into continuous and discontinuous parts as (Simo et al. 1993)

$$\dot{\boldsymbol{u}}(\boldsymbol{x},t) \;=\; \underbrace{\dot{\bar{\boldsymbol{u}}}(\boldsymbol{x},t)}_{\text{continuous}} \;+\; \underbrace{[\![\dot{\boldsymbol{u}}(t)]\!]\, H_{\mathcal{S}}(\boldsymbol{x})}_{\text{discontinuous}} \tag{1}$$

where $\dot{\boldsymbol{u}}(\boldsymbol{x},t)$ is the total velocity field, $\dot{\bar{\boldsymbol{u}}}(\boldsymbol{x},t)$ is the continuous part of the velocity field, and $[\![\dot{\boldsymbol{u}}(t)]\!]$ is the discontinuous part of the velocity field, where it is assumed here that the jump velocity $[\![\dot{\boldsymbol{u}}(t)]\!] = \dot{\boldsymbol{u}}^{+}(t) - \dot{\boldsymbol{u}}^{-}(t) = \dot{\zeta}(t)\boldsymbol{m}$ is spatially-invariant. The term $\dot{\zeta}(t)$ is the magnitude of the jump velocity, and $\boldsymbol{m}$ is its direction. $H_{\mathcal{S}}(\boldsymbol{x})$ is the Heaviside function at the discontinuity (or slip) surface $\mathcal{S}$. The singular strain rate then results as

$$\dot{\boldsymbol{\epsilon}}(\boldsymbol{x},t) \;=\; \underbrace{\boldsymbol{\nabla}^{s}\dot{\bar{\boldsymbol{u}}}(\boldsymbol{x},t) + \underbrace{\boldsymbol{\nabla}^{s}\,[\![\dot{\boldsymbol{u}}(t)]\!]}_{=\mathbf{0}} H_{\mathcal{S}}(\boldsymbol{x})}_{\text{regular}} \quad+\quad \underbrace{([\![\dot{\boldsymbol{u}}(t)]\!]\otimes\boldsymbol{n}(\boldsymbol{x}))^{s}\delta_{\mathcal{S}}(\boldsymbol{x})}_{\text{singular}} \tag{2}$$

where $(\bullet)^{s}$ denotes symmetric part, $\boldsymbol{n}(\boldsymbol{x})$ is the normal to the slip surface $\mathcal{S}$, and $\delta_{\mathcal{S}}(\boldsymbol{x})$ is the Dirac-delta function at $\mathcal{S}$. Given the resulting singular strain rate, mathematicians describe the

discontinuous velocity as belonging to the Bounded Deformation (BD) space (Matthies et al. 1979, Strang et al. 1980)

$$\dot{\boldsymbol{u}}(\boldsymbol{x},t) \;\in\; BD \tag{3}$$

which was the motivation for the seminal work by Simo et al. 1993. The term "bounded" refers to the bounded integration of the displacement gradient.

Bifurcation condition

It is assumed that upon bifurcation of material response, plastic flow is localized to the slip surface $\mathcal{S}$, and as a result the plastic consistency parameter is written as a singular distribution

$$\lambda(\boldsymbol{x},t) \;=\; \lambda_\delta(t)\,\delta_{\mathcal{S}}(\boldsymbol{x}) \tag{4}$$

where it can be shown that (Regueiro and Borja 2001)

$$\lambda_\delta(t) \;=\; \cos\psi(t)\,\dot{\zeta}(t) \tag{5}$$

where $\psi(t)$ is the angle the slip vector $\boldsymbol{m}$ makes with $\mathcal{S}$.

The bifurcation condition that allows a slip surface to form in a rate-insensitive plastically deforming material results from the requirement that balance of linear momentum must be satisfied, which in turn requires that the traction be continuous across the slip surface $\mathcal{S}$

$$[\![\dot{\boldsymbol{\sigma}}]\!]\cdot\boldsymbol{n} \;=\; \big[\!\big[\dot{\boldsymbol{t}}^{\sigma}_{\mathcal{S}}\big]\!\big] \;=\; \boldsymbol{0}\,. \tag{6}$$

This condition requires that the traction rate be regular, which leads to the bifurcation condition expressed in standard form as

$$\boldsymbol{A}\cdot\boldsymbol{m} \;=\; \boldsymbol{0} \quad\Longrightarrow\quad \det\boldsymbol{A} \;=\; 0 \quad\text{for}\quad \boldsymbol{m} \;\neq\; \boldsymbol{0} \tag{7}$$

where $\boldsymbol{A} = \boldsymbol{n}\cdot\boldsymbol{c}^{ep}\cdot\boldsymbol{n}$ is the second order elastic *perfectly*-plastic acoustic tensor. For general three dimensional stress states this bifurcation condition $\det\boldsymbol{A} = 0$ may be solved numerically by a nonlinear optimization procedure (Ortiz et al. 1987, Wells and Sluys 2001). This procedure is used to determine the time of bifurcation, slip surface normal $\boldsymbol{n}$, and slip direction $\boldsymbol{m}$ for the simple numerical example presented in this paper.

ENHANCED STRAIN FINITE ELEMENT IMPLEMENTATION

Previous model formulations (Borja and Regueiro 2001, Regueiro and Borja 2001, Borja 2002) are applicable to two and three dimensional problems. For finite element implementation, however, previous implementations must now be upgraded to account for three dimensional analysis. In particular, an enhanced strain hexahedron is formulated for implementation of this model within an assumed enhanced strain finite element method. We note that this strong discontinuity plasticity model is not restricted to this type of numerical implementation. In fact, Wells et al. 2002 have used a partition of unity approach that requires slip displacements be continuous across element faces, similar to the approach adopted by the Extended Finite Element Method (X-FEM) community (cf. Moes et al. 1999). If the partition of unity concept provides a more robust numerical algorithm, then it is clearly worth considering. Otherwise, if it is not of interest to resolve the stress within the process zone around a crack tip (i.e., for geomechanics scale problems), then the assumed enhanced strain method would seem to be adequate. Meshfree methods also lend themselves well to analyzing localized deformation problems (Liu et al. 2000) because of the choice of large domain over which the weight function may act.

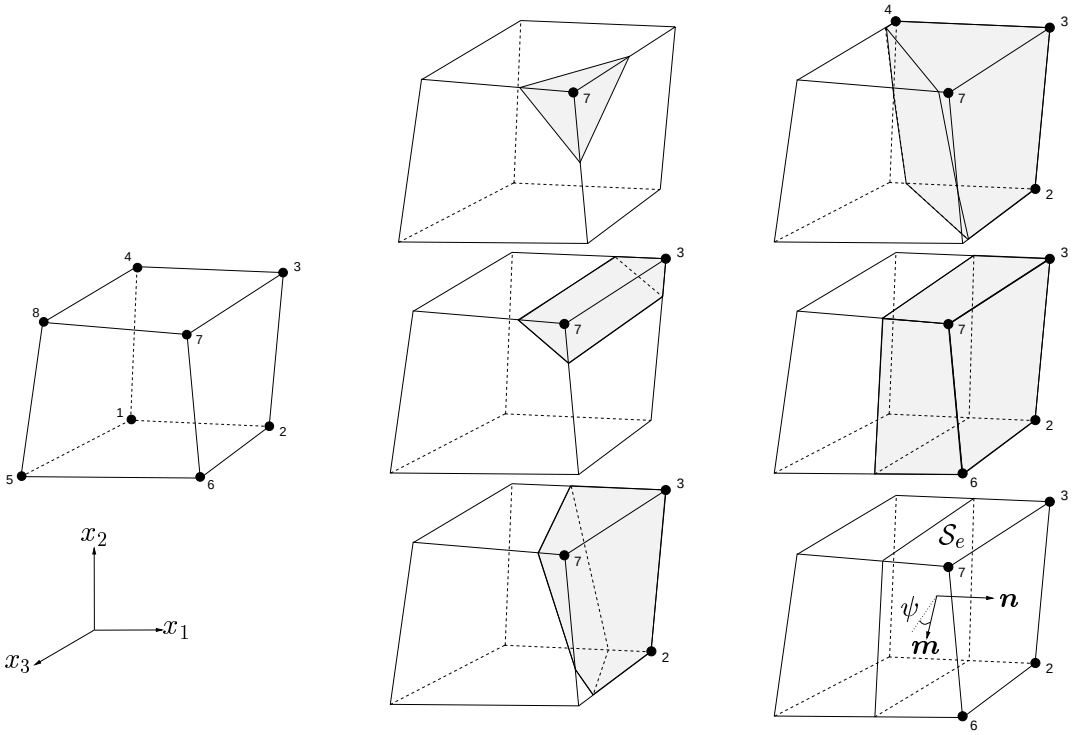

FIG. 1. Enhanced strain hexahedron with slip plane showing five possible slip-plane cutting conditions.

Details aside (Borja and Regueiro 2001, Regueiro and Borja 2001), the Cauchy stress at time t_{n+1} within a Newton-Raphson algorithm (iteration index k) is written as

$$\boldsymbol{\sigma}_{n+1}^{k+1} \;=\; \boldsymbol{\sigma}_{n+1}^{\text{trial}} \;-\; \boldsymbol{D}\cdot\boldsymbol{G}^e\,\Delta\zeta^e \quad \text{in} \quad \Omega_{\text{loc}}^e/\mathcal{S}^e \tag{8}$$

where $\boldsymbol{D}$ is the elasticity matrix, and the regular part of the enhanced strain displacement matrix $\boldsymbol{G}^e$ is

$$\boldsymbol{G}^e \;=\; [(\boldsymbol{m}^e\otimes\boldsymbol{\nabla}f^e)^s]\;. \tag{9}$$

Thus, for the enhanced strain hexahedron, it becomes a matter of determining how to construct the enhancement function f^e. Figure 1 shows the five different cutting plane conditions for the hexahedron. Figure 2 demonstrates how to determine whether a node is active in terms of constructing f^e, which then may be constructed as

$$f^e(\boldsymbol{x}) \;=\; \sum_{B=1}^{n_{\text{active}}} N^B(\boldsymbol{x})\;; \quad \boldsymbol{\nabla}f^e(\boldsymbol{x}) \;=\; \sum_{B=1}^{n_{\text{active}}} \boldsymbol{\nabla}N^B(\boldsymbol{x}) \tag{10}$$

where $N^B(\boldsymbol{x})$ is the trilinear shape function at node B.

NUMERICAL EXAMPLES

One numerical example is used to verify the numerical optimization algorithm for the plane strain case, for which we have an analytical solution for the bifurcation condition and slip line normal. The second example demonstrates the ability of the algorithm to determine bifurcation and slip surface normals for a three-dimensional boundary value problem.

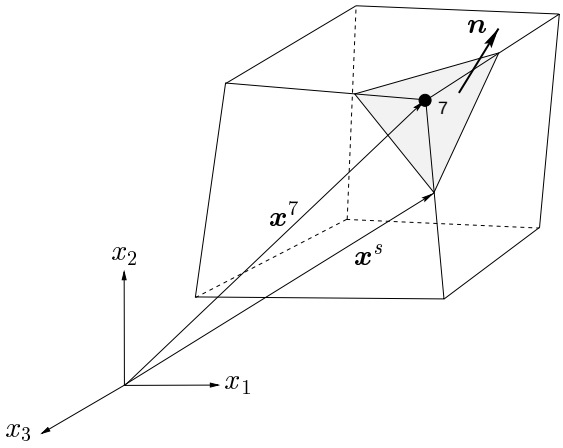

FIG. 2. Determining active nodes: if $\boldsymbol{n} \cdot (\boldsymbol{x}^A - \boldsymbol{x}^s) > 0$ then node A is active where $\boldsymbol{x}^A$ is the location of node A and $\boldsymbol{x}^s$ is the location of a point on the slip plane which has unit normal $\boldsymbol{n}$.

TABLE 1. Parameters for model

Symbol	Value
E	15 MPa
ν	0.3
cohesion $\bar{\alpha}$	13 kPa
friction β	0.5
dilation b	0.35
hard./soft. mod. H	-1 MPa

Plane strain verification

The numerical optimization algorithm is verified for a plane strain example (material parameters shown in Table 1), using eight trilinear hexahedral elements constrained in the out-of-plane direction and loaded in confined compression similar to the example discussed in Regueiro and Borja 2001. The comparison of the two numerical solutions is reasonable and is shown in Table 2.

Corner shear

The second example tests the nonlinear optimization algorithm for a three-dimensional corner shear problem shown in Fig. 3. A displacement is prescribed at the corner node $(1, 1, 1)$ with direction $\boldsymbol{d}/\|\boldsymbol{d}\| = [1, -1, 1]$. The plot of force versus magnitude of the displacement vector $\|\boldsymbol{d}\|$ is shown in Fig. 4 for the standard plasticity solution only; no post-bifurcation numerical solution is shown. The Gauss point closest to this corner node plastifies and localizes first. The resulting normals and slip directions are shown in Table 3, one of which makes physical sense, $\boldsymbol{n} = [0.57, 0.59, 0.57]$.

CONCLUSIONS

A three-dimensional extension of a previously developed two-dimensional model of pressure senstive plasticity with strong discontinuity was presented. Specifically, a numerical algorithm to detect onset of localization was demonstrated, and an enhanced strain hexahedron with

TABLE 2. Comparison of slip line and slip surface normals for 2D plane strain and 3D constrained plane strain, respectively

	2D plane strain	3D constrained plane strain
$\boldsymbol{n}$	$\begin{bmatrix} 0.84 \\ 0.54 \\ 0 \end{bmatrix}$ $\begin{bmatrix} 0.84 \\ -0.54 \\ 0 \end{bmatrix}$	$\begin{bmatrix} 0.82 \\ 0.57 \\ 0.0 \end{bmatrix}$ $\begin{bmatrix} 0.84 \\ -0.57 \\ 0.0 \end{bmatrix}$
$\boldsymbol{m}$	$\begin{bmatrix} 0.84 \\ -0.54 \\ 0 \end{bmatrix}$ $\begin{bmatrix} -0.84 \\ -0.54 \\ 0 \end{bmatrix}$	$\begin{bmatrix} 0.82 \\ -0.57 \\ 0.0 \end{bmatrix}$ $\begin{bmatrix} -0.82 \\ -0.57 \\ 0.0 \end{bmatrix}$
ψ	$24.7°$	$21.1°$

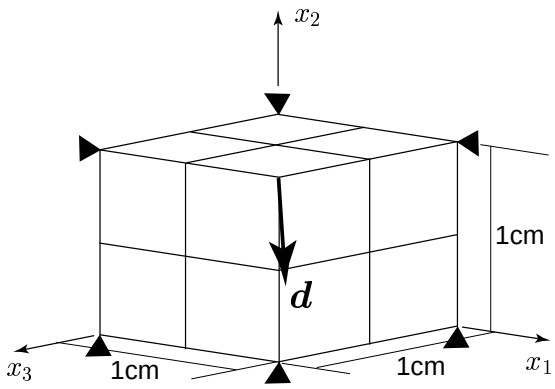

FIG. 3. Eight hexahedral element mesh with pinned corners and prescribed displacement d at one corner.

TABLE 3. Slip surface normals for 3D corner shear.

	3D corner shear
$\boldsymbol{n}$	$\begin{bmatrix} 0.57 \\ 0.59 \\ 0.57 \end{bmatrix}$ $\begin{bmatrix} 0.57 \\ -0.6 \\ 0.57 \end{bmatrix}$
$\boldsymbol{m}$	$\begin{bmatrix} 0.6 \\ -0.52 \\ 0.6 \end{bmatrix}$ $\begin{bmatrix} 0.6 \\ 0.53 \\ 0.6 \end{bmatrix}$
ψ	$22.2°$ $21.5°$

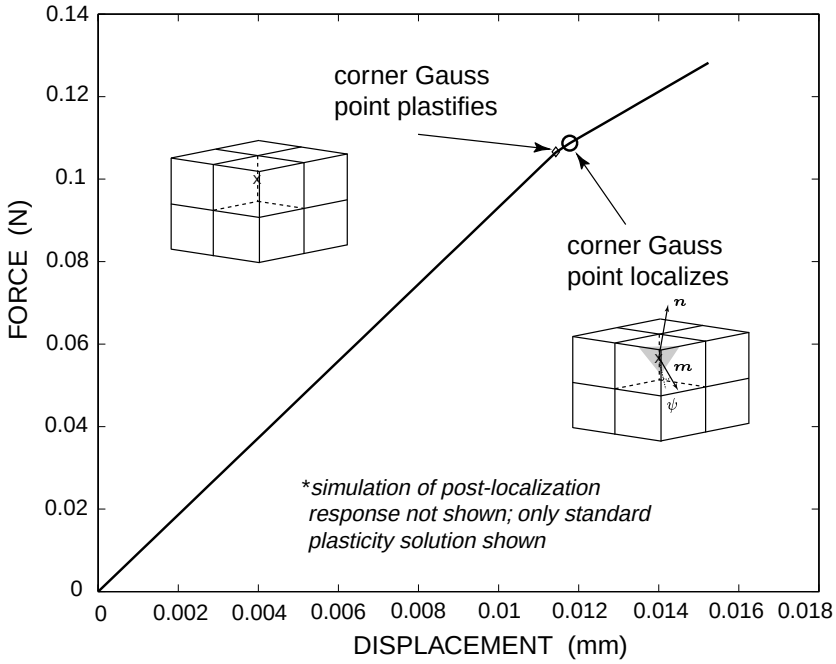

FIG. 4. Plot of force versus displacement for corner shear simulation.

slip plane was discussed. The bifurcation detection algorithm correctly predicted two unique slip normals for the contrained out-of-plane case (plane strain), and a corner shear problem also predicted two unique normals, most likely as a result of the loading symmetry. The next step is to further study the bifurcation condition and to implement the enhanced strain hexahedron in order to conduct simulations of post-bifurcation behavior.

ACKNOWLEDGEMENTS

Sandia is a multiprogram laboratory operated by Sandia Corporation, a Lockheed Martin Company, for the United States Department of Energy under contract DE-ACO4-94AL85000.

REFERENCES

Armero, F. (1999). "Large-scale modeling of localized dissipative mechanisms in a local continuum: application to the numerical simulation of strain localization in rate-dependent inelastic solids." *Mech. Cohes.-Fricct. Mater.*, 4, 101–131.

Armero, F. and Callari, C. (1999). "An analysis of strong discontinuities in a saturated poroplastic solid." *Int. J. Numer. Meth. Engng.*, 46, 1673–1698.

Armero, F. and Garikipati, K. (1996). "An analysis of strong discontinuities in multiplicative finite strain plasticity and their relation with the numerical simulation of strain localization in solids." *Int. J. Solids Struct.*, 33, 2863–2885.

Atkinson, J. (1993). *An Introduction to the Mechanics of Soils and Foundations*. McGraw-Hill.

Borja, R. I. (2002). "Bifurcation of elastoplastic solids to shear band mode at finite strain." in press.

Borja, R. I. and Regueiro, R. A. (2001). "Strain localization in frictional materials exhibiting displacement jumps." *Comput. Meth. Appl. Mech. Engng.*, 191, 2555–2580.

DiGiovanni, A., Fredrich, J., Holcomb, D., and Olsson, W. (2000). "Micromechanics of compaction in an analogue reservoir sandstone." *Proc. 4th North American Rock Mechanics Symposium*, Seattle, WA.

Hvorslev, M. (1960). "Physical components of the shear strength of saturated clays." *Research Conference on Shear Strength of Cohesive Soils*, W. Turnbull, ed., New York. ASCE, 169–273.

Larsson, R., Runesson, K., and Axelsson, K. (1996). "Localization properties of a frictional material model based on regularized strong discontinuity." *Int. J. Numer. Anal. Meth. Geomech.*, 20(11), 771–783.

Liu, W., Hao, S., Belytschko, T., Li, S., and Chang, C. (2000). "Multi-scale methods." *Int. J. Numer. Meth. Engng.*, 47, 1343–1361.

Matthies, H., Strang, G., and Christiansen, E. (1979). "The saddle point of a differential program." *Energy Methods in Finite Element Analysis*, R. Glowinski, E. Rodin, and O. Zienkiewicz, eds., New York. Wiley, 309–318.

Moes, N., Dolbow, J., and Belytschko, T. (1999). "A finite element method for crack growth without remeshing." *Int. J. Numer. Meth. Engng.*, 46, 131–150.

Needleman, A. (1988). "Material rate dependence and mesh sensitivity in localization problems." *Comput. Meth. Appl. Mech. Engrg.*, 67, 69–85.

Oliver, J., Cervera, M., and Manzoli, O. (1999). "Strong discontinuities and continuum plasticity models: the strong discontinuity approach." *Int. J. Plast.*, 15, 319–351.

Olsson, W. (2000). "Origin of luders' bands in deformed rock." *J. Geophys. Res. - Solid Earth*, 105, 5931–5938.

Ortiz, M., Leroy, Y., and Needleman, A. (1987). "A finite element method for localized failure analysis." *Comput. Meth. Appl. Mech. Engng.*, 61, 189–214.

Regueiro, R. and Borja, R. (2001). "Plane strain finite element analysis of pressure sensitive plasticity with strong discontinuity." *Int. J. Solids Struct.*, 38, 3647–3672.

Sandler, I. and Wright, J. (1984). "Strain-softening." *Theoretical Foundations for Large Scale Computations of Nonlinear Material Behavior*, S. Nemat-Nasser, R. Asaro, and G. Hegemier, eds. Martinus Nijhoff, Netherlands, 285–315.

Simo, J. and Oliver, J. (1994). "A new approach to the analysis and simulation of strain softening in solids." *Fracture and Damage in Quasibrittle Structures*, Z. Bazant, Z. Bittnar, M. Jirasek, and J. Mazars, eds. E&FN Spon, 25–39.

Simo, J., Oliver, J., and Armero, F. (1993). "An analysis of strong discontinuities induced by strain-softening in rate-independent inelastic solids." *Comput. Mech.*, 12, 277–296.

Strang, G., Matthies, H., and Temam, R. (1980). "Mathematical and computational methods in plasticity." *Variational Methods in the Mechanics of Solids*, S. Nemat-Nasser, ed. Pergamon Press, 20–28.

Wawersik, W., Rudnicki, J., Olsson, W., Holcomb, D., and Chau, K. (1990). "Localization of deformation in brittle rock: theoretical and laboratory investigations." *Micromechanics of Failure of Quasi-Brittle Materials*, S. Shah, S. Swartz, and M. Wang, eds., New York. Elsevier, 115–124.

Wells, G. and Sluys, L. (2001). "Analysis of slip planes in three-dimensional solids." *Comput. Meth. Appl. Mech. Engng.*, 190, 3591–3606.

Wells, G., Sluys, L., and de Borst, R. (2002). "Simulating the propagation of displacement discontinuities in a regularized strain-softening medium." *Int. J. Numer. Meth. Engng.*, 53, 1235–1256.